# Water infiltration through openings in a vertical plane under static boundary conditions

Nathan Van Den Bossche [1], Michael Lacasse [2], Travis Moore [2], and Arnold Janssens [1]

[1]*Department of Architecture and Urban Planning, Ghent University, Ghent, Belgium*
[2]*Institute for Research in Construction , National Research Council, Ottawa, Canada*

Keywords: watertightness, water ingress, infiltration, durability, rivulet

## ABSTRACT

An experimental setup was designed to test the effect of water deposition rate and pressure difference on the ingress of water through deficiencies. A number of round deficiencies (1mm, 4mm and 8mm diameter) were installed in a vertical polycarbonate plate, and subjected to a range of pressure differences (0, 200, 400, 600, 800Pa) and two water spray rates which are typically used in watertightness testing (2.0 and 3.4 L/min.m²). The infiltration rate was measured accurately by means of level sensors in collection troughs. This paper describes the phenomenology of the processes that govern the infiltration of water, and discusses the balance of forces that act on the water at the deficiency. The surface tension of the meniscus on the interior side of the deficiency (minus the capillary and hydrostatic pressure) defines a threshold pressure difference before infiltration will occur. The measurements confirmed the expected processes, but the pressure threshold levels for infiltration to occur supersede the calculated pressure levels. For each water spray rate the infiltration rates could be fitted to a power law, which indicates that the runoff pattern cannot be quantified as a constant hydrostatic water column.

## 1. Introduction

Moisture is the most important source of building deterioration, and rain is the prevalent source of moisture in building envelopes. Little information has been published to date on the mechanisms of water infiltration through openings in facades. A better understanding of the mechanisms that govern the water flow through openings might lead to improvement of the performance of building components towards water management, provide enhanced boundary conditions for hygrothermal simulations, and render a more scientific approach to design watertightness test protocols.

Studies related to watertightness of buildings can be differentiated into three types: (i) studies derived from investigations in the field and hence provide some insight into the significance of specific types of problems, (ii) experimental research in laboratory conditions that attempt to quantify the infiltration rates of specific components subjected to simulated climate loads, and (iii) studies that focus on designing watertightness test protocols that relate actual weathering conditions to simplified boundary conditions for performance assessment.

The information in the study by Morrison Hershfield Limited (1996) indicated that 25% of the moisture problems associated with water ingress into wall assemblies were directly attributed to penetration through the windows or the window-wall interface. Water entry testing of several different types of wall assemblies was completed in the NRC-IRC Moisture Management for Exterior Wall Systems Consortium (Lacasse et al. 2003) in which stucco, exterior insulated finish systems (EIFS), brick veneer and hardboard and vinyl siding clad assemblies were subjected to simulated wind-driven rain test conditions. In some of these assemblies, water entry through deficiencies in the cladding at location of penetration such as a ventilation duct, electrical outlet or window, was determined as a function of simulated wind-driven rain loads (i.e. pressure difference across wall specimen and water spray rate applied to the exterior cladding). Although infiltration rates were provided for a range of pressure differences and spray rates for different types of specimens, the information derived from these tests is only useful for the given size of samples, deficiencies, location of deficiencies and installation quality.

Furthermore, performance assessment of building components in a laboratory situation is typically done according to watertightness test standards, which – in most cases not mentioned explicitly – are assumed to simulate specific climatic conditions a component might be subjected to during its lifetime. According to Van Den Bossche et al. (2012), boundary conditions for watertightness testing should be based on typical failure mechanisms for that specific component, and derived from climatic analysis that takes into account the co-occurrence of rain and wind. Both peak wind pressures as well as peak rainfall intensities will depend on the averaging time. Mass buffering systems such as masonry brick walls should perhaps be tested for an extended period of time that allows saturation of the wall, which will be accompanied with more moderate pressure differences and water deposition rates due to the longer averaging time. On the other hand, face-sealed systems like some curtain wall systems that entirely rely on caulking for providing adequate performance should perhaps be subjected to peak pressure loads that only occur for a 3 second period, which will yield significantly higher pressure differences and water spray rates as compared to the test protocol for masonry brick walls. Different failure mechanisms thus require different test protocols that relate to different frequencies in wind and rain events.

Currently, little to no information has been published on the phenomenology and driving forces that characterize water ingress through openings in a vertical plane. This paper reports on experimental measurements of infiltration rates

through notional openings in a polycarbonate plate subjected to a range of pressure differences and water deposition rates. Next to that, the interacting phenomena that govern the infiltration of water through deficiencies is described and the driving forces quantified. The first three sections describe the experimental setup, the phenomenology, and the different infiltrations modes that were observed during testing. Subsequently, the results of the experiments are reported and compared to the expectations based on the balance of capillarity, surface tension and hydrostatic pressure in the deficiencies. A summary is provided in the conclusions.

## 2. Experimental setup

### 2.1 Test apparatus and specimens

An overview of the test setup is presented in figure 1. On the right there is a chamber in which the pressure can be controlled by means of a fan and a pressure actuator. The fan allows to create a static pressure difference, whereas the computer controlled electro-mechanical pressure actuator allows to impose sinusoidal pressure fluctuations with amplitudes up to 480Pa and a maximum frequency of 2Hz. The air flow generated by the fan was measured by means of a laminar flow element and the variation of pressure difference during static testing was never larger than 2.8% or 2Pa. The pressure chamber also comprised an adjustable spray rack to mount the nozzle and drainage with a siphon to avoid air losses (please refer to figure 2). The chamber consists of an aluminum frame (610mm square, 230mm deep), which was closed on one side by means of a polycarbonate plate, and a second aluminum frame which comprises the test specimen could be fixed to the other side.

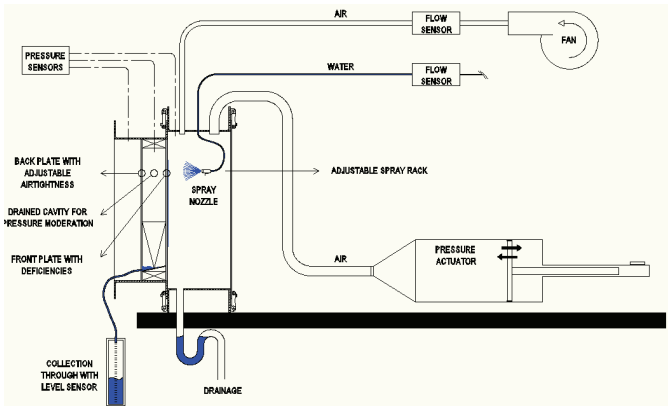


Fig. 1. Schematic of test apparatus and experimental setup

The specimen is comprised of two vertical parallel polycarbonate plates, the plates being affixed to pieces of wood of 38 mm by 100 mm. The exterior plate is exposed to the water spray and the internal plate acts as an air barrier. The cavity between external and internal plates is 100mm, and the specimen thus represents a pressure moderated façade system. Different types of openings placed in the external plate were meant to replicate the deficiencies in an external cladding; these included a series of round holes, respectively, of 1 mm (5 holes), 4 mm (4 holes) and 8 mm (3 holes) diameter, and horizontal and oblique (30° and 60° angles) slits of 2mm wide. The number and spacing of the wholes was based on the width of the uniform runoff pattern, and the minimal distance between deficiencies to minimize the risk on interaction due to flow disturbance at the deficiencies. A series of openings with varying diameters in the interior plate permitted controlling the degree of air leakage through the air barrier. Water that entered through any of the deficiencies during a test sequence was drained at the base of the assembly into a collection trough with a level sensor. The rate of water accumulation in the vessel (ml/min) was monitored continuously over the course of a test sequence such that the water entry rate in relation to pressure difference applied across the test specimen could be readily determined. This paper only reports the results for the round holes under static boundary conditions, focusing on the phenomenology of the infiltration.

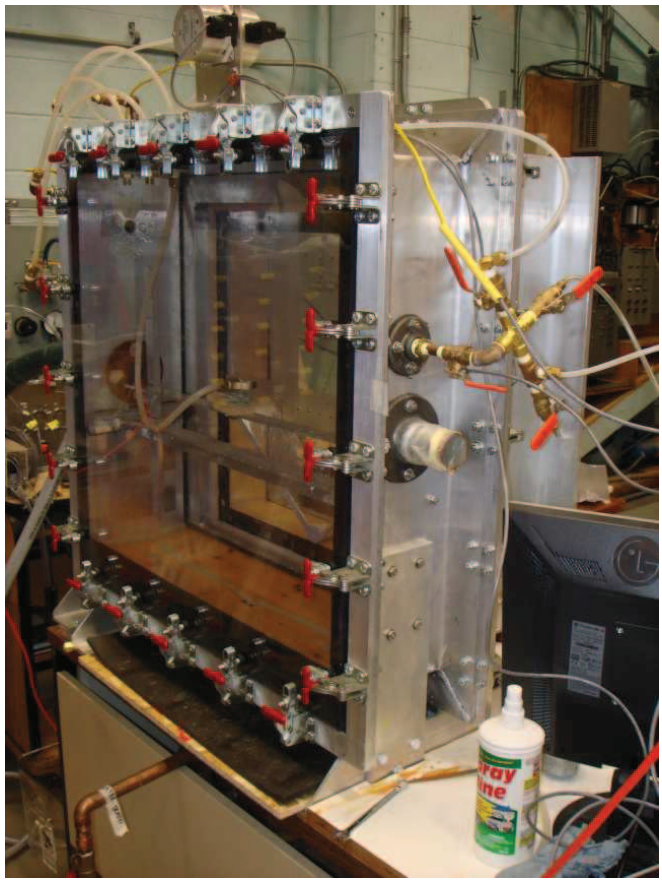

Fig. 2. Pressure chamber with flat fan nozzle and back plate with adjustable airtightness.

### 2.2 Test protocol

The test protocol consisted of: (i) undertaking pressure characterization tests on the test specimen to determine nominal test conditions to achieve the specified differential pressure across the external plate in relation to the number and size of deficiencies and air leakage conditions across the interior plate; for dynamic pressure test conditions, the frequency was also varied (ii) subjecting the deficiencies to simulated conditions of wind driven rain by means of pressure differences across and water spray onto the external plate. Spray rates used were those applied in test protocols; 2.0 L/min.m² is typical for European watertightness tests (e.g. EN 1027, 2000), whereas 3.4 L/min.m² is characteristic for North-American standard test protocols (e.g. ASTM E 2268, 2001).

Cornick and Lacasse (2009) calculated boundary conditions for watertightness testing for 5 cities in the US based on extreme value analysis (wind pressure fitted to Gumbel distribution), taking into account the co-occurrence of rain and wind. Based on that analysis the range of the test

pressures was determined (peak test value was only surpassed by the one-minute averaged value for one location for a probability of 0.99999). The test specimens were subjected to pressure differences of 0, 200, 400, 600 and 800Pa. The test program is summarized in table 1.

For the dynamic testing, the samples were subjected to the same mean pressures, but with pressure fluctuations of 20%, 33%, 50% and 80% for frequencies corresponding to 1s, 3s, 5s and 10s. The results for the infiltrations rates when subjected to dynamic boundary conditions will be reported in subsequent papers.

| Deficiencies | Water spray rate L/min.m² | Pressure difference [Pa] |
|---|---|---|
| 5 x 1mm Ø | 3.4 | 400, 600, 800 |
| 4 x 4mm Ø | 2.0 | 0, 200, 400, 600, 800 |
| | 3.4 | 0, 200, 400, 600, 800 |
| 3 x 8mm Ø | 2.0 | 0, 200, 400, 600, 800 |
| | 3.4 | 0, 200, 400, 600, 800 |

Table 1. Water entry test program under static boundary conditions.

### 2.3 Influence of nozzle types

To assess the effect of the type of nozzle, two types of nozzles were used. The first type was a full cone spray nozzle (further on referred to as cone) which is characterized by a uniform liquid distribution across a circular area, whereas the second type was a flat fan axial spray nozzle (further on referred to as flat fan) that produces a sharply defined linear spray pattern with a uniform liquid distribution. As this analysis only focuses on infiltration due to the effect of water runoff, and not the effect of direct impingement of water drops, the water spray was pointed at the location just above the deficiencies in the polycarbonate plate (lower point of impact area about 2cm above the top of the deficiency). For the cone spray, the water spray rate intensity on the specimen was determined by the water flow rate divided by the circular impact area on the specimen. To have comparable results in respect to runoff, the position of the flat fan nozzle was adjusted so that the width of the linear spray pattern was identical to the diameter of the cone spray pattern. Note that for one nozzle identical water spray rates can be achieved by simultaneously adjusting the distance to the specimen and the water flow rate.

First of all, the infiltration rates reported for the cone spray were significantly lower compared to those for the flat fan spray. The analysis is based on 10 static tests for each nozzle done for the three deficiencies of 8mm diameter, with pressure differences of 0, 200, 400, 600 and 800Pa, and water spray rate intensities of 2.0 and 3.4L/m².min. For 9 out of 10 tests, the infiltration due to the flat fan spray was on average 6.5 (standard deviation 0,9) times higher compared to the infiltration due to cone spray runoff. In one case the infiltration was 35 times higher, but this was not representative as it refers to very small absolute quantities. For the cone spray the center of the spray area was obviously further away from the deficiency itself. This distance allowed to form local rivulets of water running down the plate. The path of these rivulets meandered over the plate, and did not always cross every deficiency, and the flow pattern was very irregular. Conversely, the flat fan spray was aimed only a few centimeters above the deficiencies and thus generated a very uniform runoff that was still stable when it reached the deficiencies (without rivulets or fingering). Furthermore, when the position and spray rate of the nozzle was changed (generating the same water spray rate intensity), the flat fan nozzle proved to be more robust. Consequently, all tests reported in this paper were done with the flat fan spray.

### 2.4 Measurement error

The water that infiltrated into the construction was collected in a trough with a gravimetrically calibrated level sensor with an accuracy of 0,87% or 0.5g, whichever is greater. All reported relative errors are defined as the 95% t-distribution confidence interval derived from calibration measurements executed prior to the sample measurements. A maximum absolute error is also reported, typically derived from calibration at low levels (which would introduce significant relative errors). Pressure taps were installed in the pressure chamber as well as in the cavity between the internal and external plates. The error of the pressure sensors is limited to 4.3% or 5.6Pa, whichever is greater. The error on the water flow rate that is sprayed on the specimen is 2.6% or 0.006L/min.

However, additional tests were done to measure the repeatability of a single test. Based on three different calibration set-ups (pressure and spray rate were varied), there was a standard deviation of 16.1%, and the 95% confidence interval was 28.8%. The large discrepancy between the predicted and measured uncertainty interval can be attributed to the effect of the runoff pattern on the exterior side, which will be discussed further on.

## 3. Phenomenology

### 3.1 Runoff patterns

Before looking at the results, it is important to describe the forces and parameters that affect the infiltration of water through a deficiency, and the phenomenology of the processes that occur. There is a uniform runoff pattern that reaches the deficiencies, all of which are located on a horizontal line. Regardless whether or not infiltration occurs, the runoff pattern is affected by the deficiencies: in between the deficiencies of 4mm and 8mm the water seems to funnel into rivulets (as previously described by Paterson et al, 1995). Conversely, the runoff pattern was typically not affected by the presence of the 1mm deficiencies. The formation of rivulets is mainly determined by variations in surface roughness and local imperfections (Marshal and Wang, 2005). Obviously the water is diverted from the deficiency which will have an influence on the flow pattern, velocity and direction of the water at the holes. Although visual inspection was done during testing, it was unclear if and when the area of the deficiency was covered with water.

Note that the brim at the edge of the deficiencies caused by the drilling was sanded very carefully, together with the surrounding area (to avoid variation in surface roughness). Next to that, the surface of the polycarbonate plate was cleaned meticulously in between every test, and the

effectiveness was controlled before every test by a visual check of the uniformity of the runoff film.

The uniform film changed into rivulets at the deficiencies by forming diagonal rivulets that delimit the film runoff. The water flow at these outer boundaries is significant, whereas the water flow in between these rivulets is very shallow and in terms of flow rates less important than the rivulet (Mertens at al., 2004). Three different modes were recorded: the diagonal rivulet was typically located at the top or bottom edge of the deficiencies (figures 3 and 4 respectively), but sometimes the rivulet formation occurred below the deficiencies (figure 5). In the cases that rivulets were formed above the deficiencies, the test was stopped and repeated after cleaning the surface. These runoff patterns were typically stable for a period between 30s and 15min, but then shifted to another mode as described above. This indicates that the flow rate of the water stream lies above the dynamic flow threshold (Le Grand-Piteira et al., 2006). When the inertia of the water flow in the rivulet supersedes the pinning forces at the border the flow pattern becomes unstable and a new equilibrium is found in a different location where the pinning forces again supersede the inertia of the flow.

Although it is assumed that the runoff film introduces a pressure difference on the deficiency, it is unclear how this is affected by the different runoff patterns. Tammes and Vos (1984) claimed to find hydrostatic pressures due to runoff up to 100Pa for brick walls, but no information was provided for other substrates, and the effect of runoff patterns was not discussed. On the other hand, one can question the concept of a hydrostatic water column in a runoff film: perhaps the velocity can be high enough to introduce negative pressures on the deficiency by means of the venture effect. Furthermore, it is even uncertain whether or not water was always present at the exterior side of the deficiency. Figures 3-5 show how the location of the diagonal rivulets on the 4mm Ø deficiencies changes over time: the inertia of the water gradually overcomes the pinning forces at the edge and thus moves the rivulets downwards. However, the runoff pattern sometimes breaks up, introducing rivulets again at the deficiencies.

Fig. 3. Diagonal rivulets at the top of the deficiencies

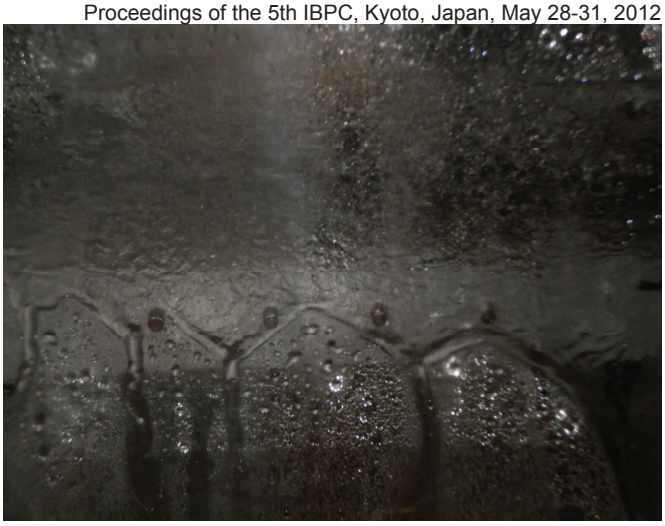

Fig. 4. Diagonal rivulets at the bottom of the deficiencies

Fig. 5. Uniform film flow over deficiencies and rivulet formation underneath

### 3.2 Infiltration

During the testing infiltration was evident for some deficiencies at specific pressure differences. During static pressure differences, water infiltrated through deficiencies, forming a rivulet at the interior side of the polycarbonate plate. In most cases this was a straight rivulet, indicating that the pinning forces supersede the lateral inertia in the water flow (flow rate below meandering threshold). During testing there was either no infiltration, drop-wise infiltration, discontinuous rivulet formation or a continuous water flow in a straight rivulet.

### 3.3 Deficiency

#### *3.3.1 Capillarity*

The size of the circular holes (1mm, 4mm and 8mm diameter) was selected on the basis of water occluding, or not, the opening by capillary action given the flow of water across the opening with smaller holes providing a greater capillary effect. Based on the Young-Laplace equation, the capillary pressure was calculated for the different diameters:

$$p_c = \frac{2\gamma \cos \vartheta}{r}$$

With $p_c$: capillary pressure (Pa), γ: surface tension of water at 10 °C (74.42 mN/m), θ: contact angle of water on substrate (according to manufacturer polycarbonate: 66°) and r: radius (m). Thus the expectation was that, given the hydrostatic pressures in the deficiencies themselves, the 1 mm diameter openings would fill with water ($p_c$ = 121Pa) whereas those of 8 mm would not ($p_c$ = 15Pa); the 4mm holes were selected as intermediate value ($p_c$ = 30Pa). The contact angle inside the deficiency was assumed similar to that of the untreated surface. However, the drilling will increase the roughness and contact angle, and consequently lower the capillary pressure, but insufficient data was found to estimate the magnitude of the effect. On the other hand, even for smooth polycarbonate plates contact angles up to 82° (Dauginet et al., 2001) are found in literature, which has a big impact on the capillary pressure. If we now conservatively assume that the roughness of the polycarbonate in the deficiency is higher due to the drilling, and consequently equal to 82° instead of 66°, the capillary pressure in the 1mm, 4mm and 8mm Ø deficiencies are 41Pa, 10Pa and 5Pa respectively.

### *3.3.2 Surface tension*

The surface tension of water will introduce a meniscus on the interior side of the front vertical plate (and perhaps on the exterior side when no water is supplied at that location due to rivulet formation). Water will only enter the cavity once the surface tension is breached by an imposed pressure, the pressure, F, calculated as follows:

$$F = \sigma * 2\pi * r$$

Where σ: surface tension of water (74.42 mN/m$^2$ at 10 °C); *r*, the wetted radius of the opening (m). Dividing F by the area of the respective deficiencies renders the equivalent external pressure difference. As a first approach, the surface of the meniscus can be considered flat, secondly, the necessary pressure is calculated assuming a spherical cap based on the contact angle at the interface (value in brackets). For the 1 mm deficiency this results in a pressure of 297 Pa (274), whereas the 4 mm and 8 mm deficiency require a pressure difference of 74 Pa (70) and 37 Pa (36) respectively. The capillary pressure and pressure to breach the surface tension are obviously linked. In isobaric boundary conditions, the meniscus formed on the interior side of the deficiency changes the contact angle and thus the capillary pressure, until there is an equilibrium with the surface tension. Consequently, when looking at only one side of the deficiency, the required pressure for infiltration to occur is the pressure to breach the surface tension minus the capillary pressure. The additional pressure will further increase the contact angle until it reaches 180°, which then corresponds to the surface tension along the perimeter of the deficiency.

### *3.3.3 Balance of forces*

The balance of capillarity, surface tension and hydrostatic pressure implies that water should not occlude larger openings such as those of 8 mm diameter and should readily flow across these openings. The hydrostatic pressure (~80Pa) is significantly higher than the pressure to breach the surface tension minus the capillary pressure (36Pa – 5Pa= 31Pa). In the case of 1 mm diameter openings, there is only a 10Pa pressure due to the water column inside the deficiency, whereas pressure to breach the surface tension is 274Pa and the capillary pressure 41Pa. Consequently, an additional (274Pa –41Pa -10Pa=) 223Pa would be necessary for infiltration to occur. For the 4mm deficiencies, the hydrostatic pressure (~40Pa) is close to the difference between capillarity and surface tension (36Pa –10Pa = 26Pa).

## 4. Infiltration modes

### 4.1 Water uptake

When water is sprayed on the exterior side of the plate, runoff will occur and due to capillary pressure water will be drawn into the deficiency. The capillary pressure only acts on one side of the hole, because at the exterior side it is still connected to the runoff and there is no contact angle that pulls on the liquid. The force that then prevents infiltration is the surface tension on the interior side, whereas capillarity, hydrostatic pressure in the deficiency, dynamic pressure caused by the runoff and exterior air pressure difference will provoke infiltration. Drawing 1 on figure 6 shows the uniform runoff pattern and the diagonal rivulet at the deficiency (in between the rivulets there is still a shallow runoff film).

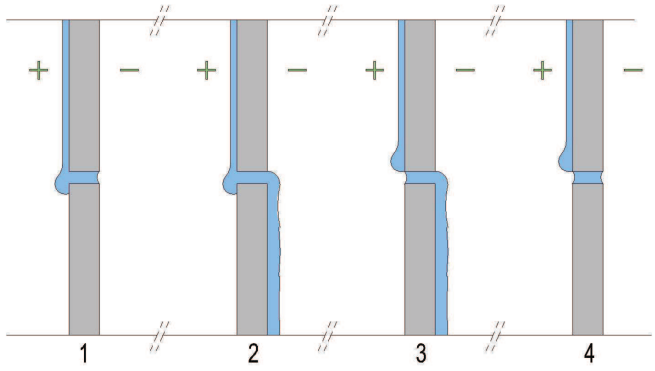


Fig. 6 Schematic representation of four infiltration modes

### 4.2 Water ingress

Once the total pressure difference is able to breach the surface tension of the meniscus, water will infiltrate on the interior side of the pane. At least one drop of water will then (partly) run down the plate, leaving a wetted trail behind. This wetted trail thus starts at the interior side of the deficiency, and will affect the buildup of a meniscus because the cohesion of the water will draw the water to the trail. Consequently, the pressure to breach the meniscus only introduces a threshold for infiltration to occur at first, and once it has been superseded the threshold is lowered due to the wetting. Depending on the infiltration rate, the infiltrated water will run down in droplets or in a continuous rivulet (straight, meandering or dynamic). Once such a rivulet is formed, the cohesive forces of the water entering the deficiency will pull on the water located inside the deficiency and hence contribute to establish a continuous infiltrating water stream. Consequently, there will be no capillary pressure in either side of the deficiency, as there is no contact angle to pull on the water.

In that case, there are no forces that prevent infiltration to occur, except for the dynamic pressure drop due to the flow in the deficiency, and the flow pattern in front of the deficiency. Based on the time-averaged infiltration rates, the velocity of the water inside the deficiencies lies in the range

0-0.008m/s, the Reynolds number then lies in the range 1-30 [-] and the pressure drop due to the friction in the tubular section of the deficiency is consequently limited to maximum 0.9Pa; and thus negligible. In order to infiltrate, the kinetic energy of the water in the runoff film needs to be compensated by the driving forces that push the water inwards. Drawing 2 of figure 6 shows the infiltration mode described above. Note that the straight rivulet on the interior side only covers a small surface due to pinning forces, and can become relatively thick in order to allow sufficient water flow rate.

### 4.3 Water supply

The measurements showed that diagonal rivulets were formed in the runoff pattern on the exterior side, located at the top, bottom or below the deficiencies. These patterns shifted during testing, altering the condition of the exterior side of the deficiency. If the rivulets were formed at the top of the hole, no water was present and the water inside the deficiency was thus subjected to an outwards oriented capillary force, whereas the cohesive forces of the rivulet are pulling the water inwards. When the capillary forces are stronger, the water will stay in the deficiency and the rivulet is stopped. It is unclear to what degree the infiltration rate affects the shift in runoff pattern on the exterior side. Figure 6 shows how the runoff pattern shifts and the diagonal rivulet moves form the bottom of the deficiency to the top of the deficiency, which corresponds to a shift from figure 4 to figure 3. It should also be noted that intermediate situations (between mode 2 and 3) occurred, and it is unclear to what degree the rivulets at the top of the deficiency were still able to provide sufficient supply.

### 4.4 Occlusion

Water can thus be trapped in the deficiency, without water supply at the exterior side, and without a rivulet at the interior side. The water inside the deficiency is then only subjected to capillary forces in both directions, the hydrostatic pressure of the water in the deficiency, and the exterior pressure difference.

## 5. Results

Test results for water entry rates through the three specified deficiencies under conditions of static pressure differential and subjected to two different water spray rates are given in Figure 7. The sequence of testing was such that those tests having nominally the largest deficiency and the highest spray were first conducted (i.e. those for deficiencies of 3 X 8 mm Ø) from the lower to the higher pressure difference; thereafter for the same deficiency, the lower spray rate was applied. As is evident from a review of the results, increasingly less water was collected at smaller deficiencies and at the reduced spray rates. Hence, no tests were conducted at a spray rate of 2 L/min-m$^2$ for the smallest deficiency (5 X 1 mm Ø) since little or no water had been collected at a pressure difference of 400 and 600 Pa at the next higher spray rate for this same deficiency size (see Table 1). Furthermore, the infiltration rates were divided by the number of deficiencies where water infiltrated during the test. For the 1mm deficiencies, water only infiltrated through 2 out of 5 deficiencies, whereas the remaining 3 were occluded all the time. For the 4mm Ø deficiencies, 2 out of 4 were occluded during testing at 3.4L/min.m² at 600 and 800Pa pressure difference. None of the 8mm deficiencies occluded during testing. The values thus represent the infiltration through one opening which is not occluded.

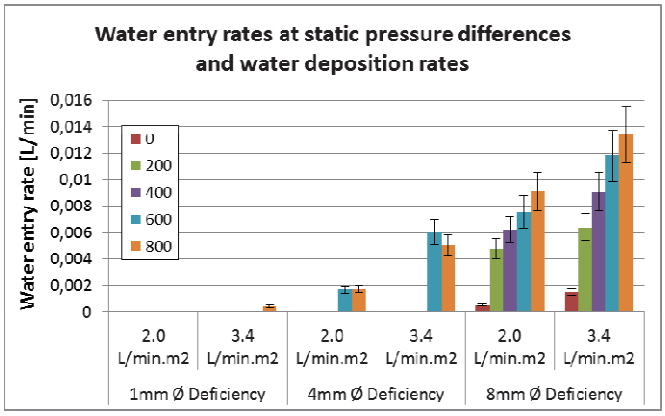


Fig. 7. Water entry rates through round deficiencies of 1mm, 4mm and 8mm diameter, subjected to static pressure differences and water deposition rates.

Increases in water entry rates were recorded for corresponding increases in pressure difference across the assembly. This is not however apparent for all test conditions but most evident for the larger deficiency of 3 X 8 mm Ø. For the 4mm deficiencies subjected to 3.4L/min.m², a higher infiltration rate was recorded at 600Pa pressure difference as compared to the test at 800Pa pressure difference. Note that this test was repeated due to the unexpected results, but the repetition confirmed the earlier findings.

The measurements confirmed – to some extent - the expected effect of capillary force and surface tension: the 1mm and 4mm Ø deficiencies were occluded at lower pressure differences, whereas the 8mm Ø deficiencies never occluded. Based on the balance of hydrostatic pressure, capillary forces and surface tension of the meniscus, it was expected that water would readily flow through the 8mm Ø deficiency without pressure difference, whereas an external pressure of 223Pa would be required for water to infiltrate the 1mm Ø deficiency. For the 4mm Ø deficiency, infiltration was expected at very low pressure differences. The results showed that water started infiltrating both the 1mm as 4mm Ø deficiency only at 600Pa, significantly higher than expected. On the other hand, the infiltration rates did differ significantly for the different size deficiencies, more in line with the expected outcome. The 8mm Ø deficiency allowed water to infiltrate without external pressure difference, and during testing no occlusion was evident. Based on the balance of forces that affect the infiltration, it was expected that the infiltration rates through the 4mm and 8mm Ø would be more similar. With regards to the infiltration rates that was the case, but the required pressure difference for water to infiltrate was much higher than expected for the 4mm Ø deficiency.

For the 1mm and 4mm Ø deficiencies insufficient infiltration rates were collected to look at trends more into detail. Figure 8 shows the infiltration rate for the 8mm Ø deficiency as a function of pressure difference (corrected for occluded openings). The data are fitted to a power law:

$$Q = C * \Delta P^n$$

with Q: infiltration rate [L/min], ΔP: pressure difference [Pa], flow exponent n equal to 0.51 (average of individual best fits), which results in flow coefficients C of 0.00029 and 0.00043L/min for spray rates 2.0 and 3.4 L/min.m² respectively. Note that the increase in water spray rate of 70% results in an increase of infiltrated water of 49%. Insufficient information was available to define the flow coefficient as a function of water deposition rate. Prior to the measurements, it was expected that the water spray rate would primarily affect the thickness of the runoff film, and likewise the pressure difference caused by the hydrostatic water column at the exterior side of the deficiency. However, figure 8 shows that the rise in deposition rate cannot be interpreted as a simple horizontal translation of the infiltration rates. Although the spray rate only affects the runoff pattern on the exterior side of the deficiency, it is remarkable that the effect is that evident and consistent in nature.

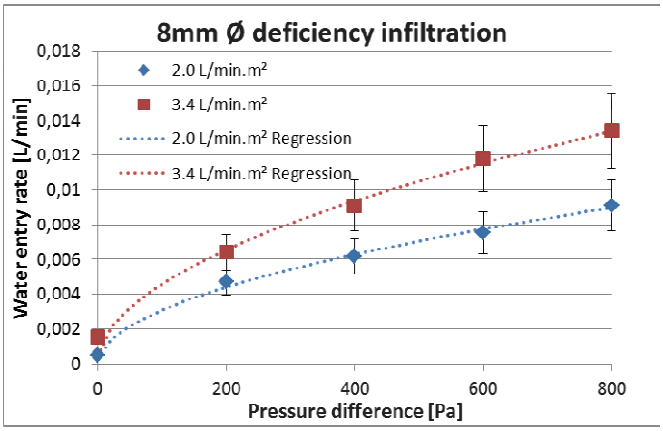


Fig. 8. Infiltration rates for the 8mm Ø deficiency: measurements and fitted power law function

## 6. Conclusions

Rain water intrusion is one of the main causes of building deterioration. Although significant research efforts have been done by the building industry on component level, the fundamentals of water infiltration through openings have hardly been studied into depth. In order to study water ingress though openings in a vertical plane under static boundary conditions, a test setup, protocol and program have been developed to test the effect of pressure difference, water spray rate, runoff pattern and type of deficiency.

The surface tension of the meniscus on the interior side of the front plate defines a pressure threshold that determines at which pressure water will enter into an assembly. When water runoff is flowing down on the exterior side of the deficiency, the contact angle of the meniscus on the interior side will change until the hydrostatic and capillary pressure in the deficiency are balanced with the surface tension of the meniscus. When infiltrating water forms a rivulet on the interior side of the deficiency, the meniscus and consequently also the capillary pressure disappears and water will easily flow through the opening. When the water supply at the exterior side stops, the capillary force will pull the water outwards, which will cause occlusion of the deficiency (if the capillary force is high enough).

Under static boundary conditions, the infiltration rate increased for rising spray rate and pressure difference. The results could be fitted with a power law function, and an increase in water spray rate of 70% resulted in an increase of the infiltration rate with 49%. More research is necessary to analyze the flow coefficient as a function of water deposition rate. The required pressure to breach the surface tension of the meniscus could to some degree explain the differences in water ingress between larger and smaller deficiencies. Based on the calculations an additional force is required for push water through the 1mm and 4mm Ø deficiencies. However, there was a discrepancy between the calculated pressures and the pressures in the experiments at which water started infiltrating.

## Acknowledgements

The authors wish to acknowledge funding for this work provided by Ghent University and the National Research Council Canada.

## References

Morrison Hershfield Limited, 1996. Survey of Building Envelope Failures in the Coastal Climate of British Columbia. Canada Mortgage and Housing Corporation, Ottawa, Canada.

Lacasse M. A., O'Connor T. J., Nunes S., Beaulieu P., 2003. Report from Task 6 of MEWS Project Experimental Assessment of Water Penetration and Entry into Wood-Frame Wall Specimens, Final Report. Research Report 133, Institute for Research in Construction, National Research Council Canada, Ottawa, Canada. (IRC-RR-133)

Van Den Bossche N., Lacasse M.A., Janssens A., 2012. Boundary Conditions for Water Tightness Testing based on Pareto-Front Analysis. Building Enclosure Science & Technology Conference. April 2-4 2012, Atlanta, US.

EN 1027, 2000. Windows and Doors – Watertightness – Test Method. CEN, Brussels, Belgium.

ASTM E 2268, 2001. Standard test method for water penetration of exterior window, skylights and doors by rapid pulsed air pressure difference. American Society for Testing and Materials, West Conshohocken, Pennsylvania, US.

Cornick S.M., Lacasse M.A, 2009. An investigation of climate loads on building façades for selected locations in the US. Journal of ASTM International. Vol. 6, No.2, pp1-17.

Paterson A., Fermigier M., Jenffer P., Limat L., 1995. Wetting on heterogeneous surfaces: experiments in an imperfect Hele-Shaw cell. Physical Review E., Volume 51, Number 2, pp 1291-1299.

Marshall J.S., Wang S., 2005. Contact-line fingering and rivulet formation in the presence of surface contamination. Computers & Fluids 34: 664-683.

Mertens K., Putkaradze V., Vorobieff P., 2004. Braiding patterns on an inclined plane. Nature, vol. 430, p165.

Legrand-Piteira N., Daerr A., Limat L., 2006. Meandering rivulets on a plane: a simple balance between intertia and capillarity.Physical Review Letters 96, No. 254503.

Tammes, E., Vos, B.H. (1984). Warmte- en vochttransport in bouwconstructies (*Heat and Moisture Transport in Building Construction*). Kluwer Technische Boeken B.V. – Deventer, Antwerp, Belgium.

Dauginet L., Duwez A.-S., Legras R., Demoustier-Champagne S., 2001. Surface modification of polycarbonate and polyethyleneterephthalate films and membranes by polyelectrolyte deposition. Langmuir, Vol 17, No. 13, pp 3952-3957.